Title

Characterization of Cardiac Pericyte Proliferation and Function Following a Myocardial Infarction

Author

Shih, Kevin Daniel

Publication Date

2022

UNIVERSITY OF CALIFORNIA

Los Angeles

Characterization of Cardiac Pericyte Proliferation and Function Following a Myocardial Infarction

A thesis submitted in partial satisfaction

of the requirements for the degree Master of Science

in Physiological Science

by

Kevin Daniel Shih

2022

ABSTRACT OF THE THESIS

Characterization of Cardiac Pericyte Proliferation and Function Following a Myocardial Infarction

by

Kevin Daniel Shih

Master of Science in Physiological Science

University of California, Los Angeles, 2022

Professor Pearl Jennine Quijada, Chair

Background: Pericytes are abluminal mural cells implicated in angiogenesis, remodeling, stabilization, and maturation of microvasculature in the brain, lungs, kidneys, and retina. These cells have been reported to dissociate from the surrounding microvasculature following an ischemic injury. However, little information is known about cardiac pericyte migration and proliferation following a myocardial infarction (MI).

Methods: CSPG4$^{CreERT2/+}$;Rosa26 Ai9$^{tdT/+}$ mice were used to measure pericyte migration and proliferation following a MI time course. CSPG4$^{CreERT2/+}$;p53$^{flox/flox}$ mice were used to measure the impacts of knocking out p53 within pericytes under healthy and MI conditions.

Results: Cardiac pericytes increase in size starting at 7-days post-injury and undergo peak proliferation at 14-days post-injury. Cardiac pericytes reached peak migration at distances

>45µm 7-days post-injury. No phenotypic differences were observed between p53 KO and WT pericytes at baseline.

Conclusions: Increases in pericyte proliferation and migration at later time points could indicate that pericytes contribute to the pro-reparative response in the heart after MI.

Graphical Abstract

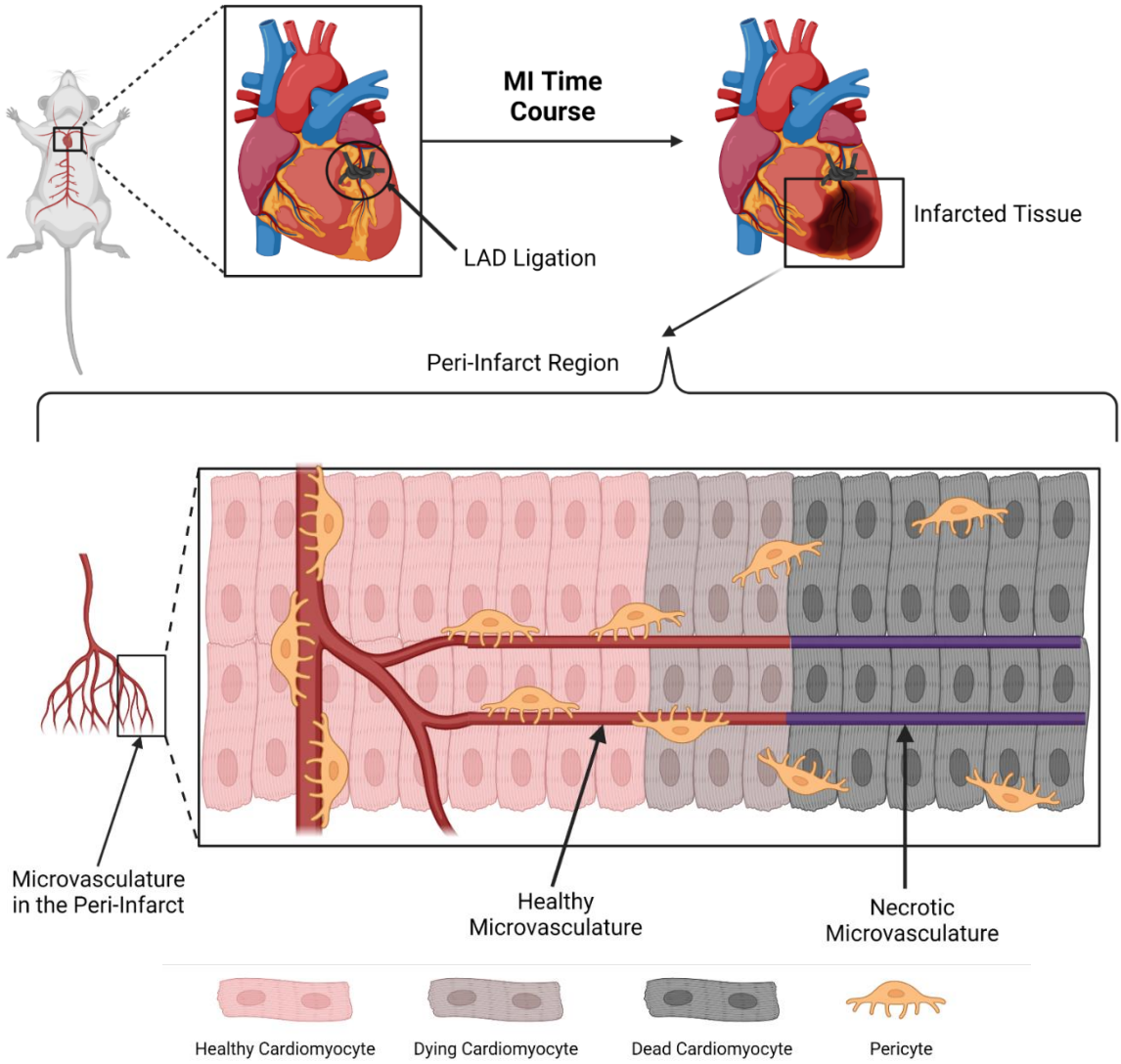

The thesis of Kevin Daniel Shih is approved.

Reza Ardehali

Rachelle Hope Crosbie

Pearl Jennine Quijada, Committee Chair

University of California, Los Angeles

2022

TABLE OF CONTENTS

LIST OF FIGURES AND TABLES

ABBREVIATIONS / ACRONYMS

AA = Abdominal Aorta

αSMA = α Smooth Muscle Actin

BrdU = Bromodeoxyuridine

BW = Body Weight

BZ = Border Zone

CM = Cardiomyocyte

COL1A1 = Collagen 1A1

CSPG4x = Chondroitin Sulfate Proteoglycan 4 with a Cre site for recombination; specific to pericytes

Dα = Donkey Anti-

DAPI = 4',6-diamidino-2-phenylindole

Dex-Bio = Biotinylated Dextran

DPBS = Dulbecco's Phosphate Buffered Saline (sterile)

EC = Endothelial cells

HW = Heart Weight

IB-4 = Isolectin

IVC = Inferior Vena Cava

IZ = Infarct Zone

Ki-67 = Nuclear protein Ki-67 indicating proliferation

LAD = Left Anterior Descending Artery

LV = Left Ventricle

MI = Myocardial Infarction

NG2 = Neuron Glial Antigen 2 (also known as Chondroitin Sulfate Proteoglycan 4)

PC = Pericyte

PCNA = Proliferating Cell Nuclear Antigen

PDGFRβ = Platelet-Derived Growth Factor Receptor β

PECAM-1 = Platelet Endothelial Cell Adhesion Molecule – 1

POSTN = Periostin

R26 = Rosa26 Ai9$^{tdTomato/+}$

RGS5 = Regulator of G-Coupled Protein Signaling – 5

RZ = Remote Zone

SMC = Smooth Muscle Cells

TAM = Tamoxifen

tdT = tdTomato

Tgfβr1/TGFβR1 = Transforming Growth Factor Beta Receptor 1 Gene/Protein

TL = Tibia Length

VEGF(R1) = Vascular Endothelial Growth Factor (Receptor 1)

vSMC = Vascular Smooth Muscle Cells

ACKNOWLEDGEMENTS

First and foremost, I would like to acknowledge my PI, Dr. Pearl Quijada, who has been an incredible mentor to me. Over the past two years Dr. Quijada has fostered a safe and encouraging environment for me to learn and grow as a scientist; and it is largely due to her that I have decided to pursue my interests in research and education so that I may inspire others as she has inspired me. Thank you Dr. Quijada for all of your time, lessons, wisdom, and support.

I would also like to acknowledge my family for all their love and support over the past two years. Thank you for supporting me in my goals and dreams.

I would also like to acknowledge each member of the Quijada Laboratory for all of their support in my research: David Wong, Julie Martinez, Matthew Tran, Maya Cornejo, Jessica Tsui, and Amy Lefley.

I would also like to acknowledge my thesis committee for all of their assistance, suggestions, and support in my research and academic growth. Thank you, Dr. Reza Ardehali, Dr. Rachelle Crosbie, and Dr. Pearl Quijada.

And finally, I would like to acknowledge the Integrative Biology and Physiology Class of 2022 for all their encouragement, support, and dedication to furthering the knowledge and understanding of their respective fields. Despite all of the trials and tribulations we faced during the beginning of the COVID-19 pandemic, the Class of 2022 perservered and helped create an amazing experience throughout this program.

SIGNIFICANCE

Treatments for myocardial infarctions are extremely limited in effectiveness due to the limited regenerative abilities of the post-mitotic adult heart (Avolio & Madeddu, 2016; Frangogiannis, 2019; Prabhu & Frangogiannis, 2016; Xin et al., 2013). Current treatments revolve around re-perfusing the infarcted region but are often quite invasive, have limited success, and require multiple treatments for sustained efficacy, such as stents (Stevens et al., 2021). However, pericytes have been proposed as a potential treatment for MIs due to their pro-angiogenic roles under homeostasis (Attwell et al., 2016; Bergers & Song, 2005; Gonzales et al., 2020; Konstantin Stark, 2018; Su et al., 2021). Pericytes are abluminal mural cells implicated in the processes of angiogenesis, microvascular remodeling, stabilization, and maturation under homeostatic conditions (Alex & Frangogiannis, 2019; Attwell et al., 2016; Avolio & Madeddu, 2016; Bergers & Song, 2005; Cai et al., 2017; Murray et al., 2017; Su et al., 2021). Pericytes are also known to aid in the regulation of vasoconstriction and vasodilation within the microvasculature (Lee et al., 2021). However, it is currently unknown how pericytes will respond following a MI. To better understand the therapeutic potential of pericytes, our research aims to characterize pericyte migration, morphology, and proliferation following a MI time course.

INTRODUCTION

Pericyte Biology

Pericytes are abluminal mural cells that surround precapillary arterioles, capillaries, and venules using a series of cellular processes extending from their cell body (Attwell et al., 2016; Avolio & Madeddu, 2016; Bergers & Song, 2005). These processes serve to regulate microvascular permeability by controlling vasoconstriction and vasodilation by means of contraction and relaxation using α-smooth muscle actin (αSMA) (Attwell et al., 2016; Brown et al., 2019; Hamilton, 2010). Believed to originate from mesenchymal cells, pericytes and their projections adhere to the endothelial basement membrane of the microvasculature by means of tight junctions; and will also communicate to surrounding cells using paracrine signaling via gap junctions (Avolio & Madeddu, 2016, DeLisser 2006, Yamamoto, Muramatsu et al. 2017, Lee, Khakoo et al. 2021). Pericytes are located in the brain, liver, kidneys, heart, retina, bone marrow, skeletal muscle, and adipose tissue (Avolio & Madeddu, 2016). However, pericyte density is dependent on tissue type and localization within the tissue (Avolio & Madeddu, 2016). While it is suspected that pericytes are heterogeneous cells that function differently depending on tissue type, studies to identify pericytes are limited (Attwell et al., 2016; Avolio & Madeddu, 2016; Bergers & Song, 2005; Lee et al., 2019; Murray et al., 2017; Su et al., 2021; Su et al., 2018).

Pericyte Identification

One of the main challenges with pericyte-based research is identifying these cells due to their heterogeneity and similarities in genetic and protein expression with other cell types (mainly endothelial cells and vascular smooth muscle cells [vSMC]) (Attwell et al., 2016; Avolio & Madeddu, 2016; Bergers & Song, 2005; Lee et al., 2019). Some of the genes and proteins that have been used to label pericytes are as follows:

- Aminopeptidase A and N (membrane-bound proteins)
- αSMA (α smooth muscle actin)
- Calponin (SMC-specific thin filament protein)
- CD31 (platelet endothelial cell adhesion molecule; PECAM-1)
- CD146 (melanoma cell adhesion molecule; MCAM)
- Connexin-43 (proteins expressed in gap junctions)
- Desmin (muscle-specific class III intermediate contractile filaments found in skeletal, cardiac, and SMC)
- Nestin (marker for neural stem cells)
- NG-2 (neuron-glial antigen 2; chondroitin sulfate proteoglycan – 4 [CSPG4])
- PDGFRβ (Platelet-derived growth factor receptor β)
- RGS5 (regulator of G protein signaling – 5)
- *XlacZ4* (a promoter trap transgene)

(Armulik et al., 2005; Attwell et al., 2016; Avolio & Madeddu, 2016; Bergers & Song, 2005; Brown et al., 2019; Chen et al., 2017; D'Amore & Sakurai, 2006; DeLisser, 2006; Hsieh et al., 2006; Kim et al., 2015; Lee et al., 2019; Orlich et al., 2022; Pham et al., 2021; Su et al., 2021;

Tucker et al., 2020; Xin et al., 2013). However, not all of these genes and proteins will be expressed in all pericytes, and relative expression will vary upon the location in the body (Armulik et al., 2005; Avolio & Madeddu, 2016; Bergers & Song, 2005). To combat the heterogeneity in gene and protein expression, combinations of the aforementioned genes and proteins can be used to label pericytes, such as $CD34^{+}$;$CD31^{-}$;$CSPG4^{+}$ in the post-natal adult heart (Avolio & Madeddu, 2016). While combinations of cell type markers are not required to study pericyte role and function, they will provide more accurate results in distinguishing pericytes from other cell types such as ECs and vSMCs.

Pericyte Roles Under Homeostasis

Pericytes play a significant role in maintaining the microvascular blood flow in various tissues of the body (D'Amore and Sakurai 2006, DeLisser 2006, Attwell, Mishra et al. 2016, Pham, Park et al. 2021). Functioning in a similar manner to the smooth muscle cells surrounding larger blood vessels, pericytes utilize finger-like projections composed of contractile filaments to regulate vasoconstriction, vasodilation, and permeability within the microvasculature in response to both cholinergic and adrenergic signaling (Avolio & Madeddu, 2016; Bergers & Song, 2005). Pericytes have also been implicated in angiogenesis by assisting in the formation, remodeling, stabilization, and maturation of blood vessels (Bergers and Song 2005, Frangogiannis 2014, Alex and Frangogiannis 2019). In response to vascular endothelial growth factor (VEGF) signaling (causes the release of proteases to deteriorate the adhesion proteins connecting the endothelial cells (EC) together) and other angiogenic signals, pericytes will mediate EC expansion into the surrounding tissue to form new blood vessels (Armulik et al., 2005; Bergers & Song, 2005;

D'Amore & Sakurai, 2006; Eilken et al., 2017). Pericytes have also been shown to produce extracellular matrix proteins (ECM) in the liver (Bergers & Song, 2005). However, the variation in pericyte roles largely depends on tissue type (Bergers & Song, 2005). Because of the pro-angiogenic potential that pericytes possess, Investigators have started to consider pericytes as a potential therapy for ischemic-related injuries.

Pericytes as a Potential Therapy for Ischemic-Related Injuries

Treatments to reperfuse tissue following ischemic damage are largely ineffective, therefore, pericytes may serve as a potential therapy due to their angiogenic properties (Alex & Frangogiannis, 2019; Avolio & Madeddu, 2016; Bahit et al., 2018; Bergers & Song, 2005; Cai et al., 2017; Eilken et al., 2017; Frangogiannis, 2019; Hsieh et al., 2006; Lee et al., 2021; Murray et al., 2017; O'Farrell & Attwell, 2014; O'Farrell et al., 2017; Pham et al., 2021; Su et al., 2021; Xiaojuan Su, 2019; Xin et al., 2013). Under pathological conditions in the brain, pericytes have been observed to disassociate from the surrounding microvasculature and migrate towards the infarcted regions (Brown et al., 2019; Fernández-Klett et al., 2010; Frangogiannis, 2019; Pham et al., 2021; Xiaojuan Su, 2019). However, contrary to the belief that pericytes may induce angiogenesis as a pro-reparative response once they reach the infarcted regions in the brain, pericytes have been found to adopt a more pro-fibrotic response and increase expression of periostin (POSTN) and collagen 1A1 (COL1A1) – ECM proteins that are common indicators of fibrosis (Brown et al., 2019; Pham et al., 2021). However, other studies suspect that pericytes may secrete ECM proteins as a means of "reparative fibrosis" to maintain tissue structure while local immune cells remove the damaged tissue (Avolio & Madeddu, 2016). This contradiction in

information requires more investigation to be done to fully understand the potential roles that pericytes may possess. Pericytes have been largely characterized in other regions of the body under both homeostatic and pathological conditions, but limited knowledge on pericyte function within the heart exists (Avolio & Madeddu, 2016; Bergers & Song, 2005; Pham et al., 2021).

Pericyte Characterization

As demonstrated in Pham, et al., 2021 in the brain, when the tissue is subjected to ischemic conditions, the pericytes will disassociate from basement membrane of the microvasculature, migrate into the infarcted region, and secrete extracellular matrix proteins (Pham, Park et al. 2021). Given this information in conjunction with previous studies, we suspected that pericytes would behave similarly in the heart when subjected to a MI (Cai, Liu et al. 2017, O'Farrell, Mastitskaya et al. 2017, Alex and Frangogiannis 2019, Lee, Khakoo et al. 2021). To study pericyte behavior with respect to migration and proliferation, we subjected CSPG4CreERT2/+;Rosa26 Ai9tdT/+ mice to MI surgery following tamoxifen administration. We hypothesized that pericyte relocation into the infarct is in response to inflammatory or angiogenic cues released from the damaged myocardial and vascular tissue; and that pericytes will undergo increased proliferation following the generation of these cues. Once the pericytes enter the infarct, we suspect that these cells will aid in the process of interstitial tissue reformation through the secretion of extracellular matrix factors and pro-inflammatory cell recruitment to mediate fibrotic remodeling and vascular recovery. Furthermore, we were also interested in the impacts of disrupting the cell cycle regulator p53 within pericytes on their migration, morphology, and proliferation following a MI. We hypothesized that the functional deletion of p53 within the pericytes would result in rapid proliferation of the pericytes near the

infarct border. We also suspect that the rapid proliferation of the pericytes will initially result in increased angiogenesis as a cardiac reparative response followed by an expansion of the fibrotic tissue due to the ability of pericytes to produce extracellular matrix proteins. The results of this study will provide information on both pericyte function within the heart in response to an injury as well as its potential as a therapeutic solution for damaged cardiac tissue repair.

MATERIALS AND METHODS

Mouse Models

For Aim 1, we utilized CSPG4$^{CreERT2/+}$; Rosa26 Ai9$^{tdTomato/+}$ mouse models for the MI time course experiments. These mice were subjected to tamoxifen injections for 7 days and then separated into injury and non-injury groups. Mice within the non-injury group did not undergo a MI. Mice within the injury group received MI surgeries and then were sacrificed at specific time points. Heart, lung, brain, and kidney were harvested at the following time points: 1 day, 3 days, 5 days, 7 days, 10 days, 14 days, and 28 days post-MI. At each indicated time-point, mice were injected with bromodeoxyuridine (BrdU), a thymidine analog that incorporates DNA into dividing cells to assess for cell proliferation. Additionally, mice were administered fluorescently conjugated Isolectin and Biotinylated Dextran via lateral tail vein injection to label cardiac vasculature. Following our limited success of Isolectin and Dextran incorporation through tail vein injections, we transitioned to injecting the mouse models through the ventral tail artery.

For Aim 2, CSPG4$^{CreERT2/+}$; p53$^{flox/flox}$ mouse models were utilized. These mice were subjected to tamoxifen injections for 7 days and will then be separated into control (CSPG4$^{CreERT2/+}$; p53$^{+/+}$) and experimental (CSPG4$^{CreERT2/+}$; p53$^{flox/flox}$) groups. Mice within the control group and experimental group will be subjected to MI, analyzed for systolic and diastolic function using echocardiography (VEVO 3100 housed in the Terasaki Life Sciences Vivarium), and then sacrificed at specific time points. To determine if p53 deletion in pericytes alters cardiac morphology without a pathophysiological stimulus, we will monitor both control (p53 wild type) and experimental (p53 KO) mice by echocardiography. Heart, lung, brain, and kidney will be harvested at the following time points: 1 day, 3 days, 5 days, 7 days, 10 days, 14 days, and 28 days post-MI. As described in Specific Aim 1, mice will be injected with BrdU and

Isolectin, and tissues will be cryosectioned. Pericytes, vasculature and proliferation will be visualized using confocal microscopy. Pericyte migration, morphology, and proliferation will be quantified using Imaris v9.8.

Injections

Tamoxifen Injections

Tamoxifen purchased from Sigma Aldrich (T5648, dry powder, stored at 4ºC) was dissolved in Sunflower seed oil (Sigma Aldrich, S5007, stored at RT in the chemical alcove) at a concentration of 10mg/mL. Tamoxifen was administered at a dosage of 100 mg/kg by intraperitoneal injection in 6-8-week-old mice once per day (every 24 hours) for 7 consecutive days.

BrdU Injections

To label proliferating cells in the heart, mice were injected intraperitoneally with BrdU at a dosage of 50mg/kg. The mice were sacrificed 4 hours later, and the hearts were processed for immunofluorescence staining as described below.

Tail Vein/Artery Injections (Biotin-Dextran and Isolectin [IB-4])

Prior to sacrificing animals, mice were administered Isolectin GS-IB4 (0.25ug/mouse) and Dextran Biotin 70,000 MW (25mg/mouse) via injection into the ventral tail artery and mice were allowed to rest for at least one hour prior to harvesting of tissue.

Myocardial Infarction

Mice were anesthetized by exposure of isoflurane/oxygen mixture and intubated with a 20-gauge angiocath and ventilated with a volume-cycled rodent ventilator at 130 cycles/min (SAR-830, CWE, Inc). After left thoracotomy between the fourth and fifth rib, the pericardium was opened, and the left anterior descending coronary artery (LAD) was ligated intramurally 1-2 mm from the tip of the normally positioned left atrium with an 8-0 suture. Lungs were reinflated and the chest was closed in two layers; the ribs (inner layer) were closed with 6-0 coated vicryl sutures in an interrupted pattern. The skin was closed using 6-0 nylon or silk sutures in a subcuticular manner. Ventilation was maintained until sufficient spontaneous breathing occurs, and the mice were allowed to recover in a temperature-controlled chamber until they resumed full alertness and mobility.

Echocardiography

Prior to performing the echocardiogram, the hair from the ventral portion of the torso was removed from the mice using Nair Hair Removal Lotion with Soothing Aloe & Lanolin. The mice were then exposed to VET ONE Fluoriso (Isofluorane, USP), a general anesthetic that induces sleep and was maintained throughout the entirety of the procedure to ensure a constant heart rate of approximately 400 bpm. Using the Vevo 3100 Echocardiogram and micromanipulator platform measuring the electrophysiologic and myocardial structure-function by FujiFilm | Visual Sonics, the following data was obtained from the long axis, short axis, and 4-chamber views: heart rate, systolic and diastolic diameters of the left ventricle, systolic and diastolic volumes of the left ventricle, stroke volume, ejection fraction, fractional shortening, cardiac output, and mass of the left ventricle **(Supplementary Figure 1)**. Within the 4-chamber

view, the pulse wave doppler and tissue wave doppler were utilized to obtain data on the diastolic function of the heart. Echocardiography was performed at baseline and over a longitudinal time course to evaluate cardiac function and recovery from surgical procedures. This data was analyzed using the Vevo LAB software and then exported to an Excel spreadsheet for further analysis. Signa Gel was used on the electrodes to ensure high conduction and Aquasonic Clear ultrasound gel was utilized for the ultrasound probe. Transpore tape was used to restrain the mouse in place and VetEquip Vapor Guard was used to reduce the toxicity of the Isofluorane.

Tissue Perfusion, Isolation, and Fixation

Before conducting an abdominal aortic retro-perfusion non-survival surgery on the mice, the mice were given an injection of approximately 300-400µL of a Ketamine-Xylazine mixture (1.3mL of Zetamine Ketamine Hydrochloride [100mg/mL] + 0.44mL AnaSed Xylazine Injection [20mg/mL] + 8.26mL sterile DPBS) intraperitoneally to serve as both a sedative and analgesic. The abdominal region of the mouse was then gently cut open **(Supplementary Figure 2)** to expose the internal organs. A cotton-tipped probe was utilized to shift the internal organs to one side and expose the inferior vena cava (IVC) and the abdominal aorta (AA), found laterally towards the mouse's left side of the IVC. Utilizing suturing thread and both strong-curve and straight tweezers, a square knot was tied around the caudal region of the IVC and AA before they branch to the lower extremities. Connective tissue around the IVC and AA was removed to provide space for a clamp to be placed on the IVC and AA near the liver and kidneys, thus effectively preventing uncontrolled blood loss from arterial lesions. Using micro-scissors, a half-moon cut was made in the AA between the suture and clamp and then a cannula was inserted

into the AA. The cannula was then secured in place by transferring the clamp from the IVC/AA to on top of the cannula and a syringe with DPBS was connected to the cannula. Prior to injecting the DPBS into the cardiovascular system, a small incision was made on the caudal portion of the IVC to allow for blood and excess fluid drainage and prevent unwanted ruptures in the cardiovascular system. Following the DPBS injection, a relaxation buffer containing potassium chloride (KCl) was injected to stop the heart from beating – thus sacrificing the mouse. The cannula was then connected to a hypertonic 0.9% sodium chloride IV for 5 minutes and then transferred to receive neutral buffered formalin (NBF) for 15 minutes to completely fix the tissue. The heart weights and tibia lengths were measured and then the hearts, lungs, kidneys, and brains were collected from the mice and stored in formalin for 16-24 hours. The tissues were then transferred to 10%, 20%, and 30% serial dilutions of sucrose in PBS for 24 hours respectively and stored at 4ºC. This was done to remove as much water from the tissues as possible and prevent cracking and crystallization formation when frozen.

Tissue Embedding and Cryosectioning

Following the tissue fixation in formalin and the serial dilutions of sucrose, the tissue was placed in a cryosectioning mold and then embedded in Optimal Cooling Temperature (OCT) media and then frozen above a combination of liquid nitrogen and dry ice. Once the tissue was completely frozen, the tissue was stored at -80ºC until ready to be sectioned. Using the Leica CM 3000 cryostat, the tissue was sectioned at a thickness of 25µm and placed on SuperFrost Gold Plus slides and stored at -20ºC.

Immunohistochemistry Staining

Protocol

For immunofluorescence staining, slides were left at room temperature for 10 minutes, washed 3 times with PBS (for 5 minutes each time), and permeabilized with 0.2% Triton X-100 (prepared in PBS) for 30 minutes. Slides were then washed briefly with PBS and an Immedge Hydrophobic pen was used to outline the staining area (sections closer to the label were designated as experimental and sections farther away were used as the controls). Slides were then treated with a blocking buffer (10% Donkey Serum in PBS) for 30 minutes at room temperature, followed by incubation with primary antibodies (diluted in blocking buffer at 1:100) overnight at 4°C in the dark. The next day, slides were washed 3 times with PBS (for 5 minutes each time) and incubated with secondary antibodies (Thermo Fisher Scientific) diluted in a blocking buffer at 1:100 for 1 hour at room temperature. After another 3 washes with PBS for 5 minutes each time, DAPI (1mg/mL) was added to the slides at a dilution of 1:2000 for 5 minutes at room temperature. Coverslips were mounted on the slides using Vectashield Plus Antifade Mounting Medium for preliminary experiments and Prolong Diamond Antifade Mountant from Thermo Scientific for the following experiments.

Preliminary Data Staining

Prior to sacrifice, the CSPG4$^{CreERT2/+}$; Rosa26 Ai9$^{tdTomato/+}$ mice (also used for the study presented in Quijada et al., 2022) were injected with Biotinylated Dextran antibodies and Isolectin (IB-4) through a tail-vein injection (TVI). A Streptavidin Alexa Fluor 488 Conjugate secondary antibody was used to visualize the Dextran and 4',6-diamidino-2-phenylindole (DAPI)

was used to visualize the nuclei. Due to the genetics, the pericytes would auto-fluoresce tdTomato at 555nm.

Picro Sirius Red Staining Protocol

To visualize collagen within an injured heart, we utilized a Picro Sirius Red F3Ba stain kit from Polysciences Inc. The proposed protocol was designed for staining paraffin sections rather than frozen sections and thus the protocol had to be modified. Our revised protocol for staining IHC-F slides were as follows: to begin, slides were removed from the -20°C freezer and allowed to thaw for 30 seconds. The sections were then hydrated with distilled water for 10 seconds, water was then removed and then Picro Sirius red stain was added to the slides for 20 minutes without disturbance. Following the 20-minute incubation, Picro Sirius red stain was rinsed with hydrochloric acid for 1 minute twice. Following the second hydrochloric acid incubation and rinse, slides were placed in 70% Histology-grade ethanol for 3 minutes, followed by placement of slides in 100% Histology-grade ethanol for 3 minutes. Following ethanol incubation, slides were set to dry for approximately 30 seconds prior to application of Permount and a cover slip. Stained slides were imaged by bright field imaging and tile scanned at a magnification of 20x using the Applied Imaging Leica Aperio Verso scanner. Quantitation of Picro Sirius was performed using Image J Version 2.0. software (National Institutes of Health, USA) by normalizing the area of Picro Sirius stain to the area of the left ventricular free wall.

Proliferation Data Staining

Cellular proliferation was visualized using BrdU, Ki-67, and PCNA for Specific Aim 1. For stains utilizing BrdU, a Rat monoclonal BrdU antibody as well as Isolectin (IB4) was

injected via TVI and allowed to circulate for approximately 4 hours prior to sacrificing the mouse. A Donkey Anti-Rat Alexa Fluor 488 secondary antibody was then utilized to visualize the cellular proliferation. Rabbit ERG primary antibodies were utilized to label the nuclei of endothelial cells.

Immunohistochemistry Imaging

IHC imaging was conducted on the ZEISS LSM 880 or LSM 700 confocal microscopes from the UCLA Broad Center of Regenerative Medicine & Stem Cell Research Microscopy Core. Zen (black edition) software was used to image the slides and Zen (blue edition) software was used for image processing. Adobe Illustrator and Photoshop were used in image processing and figure organization.

Immunohistochemistry Analysis

IHC image analysis was done on Imaris version 9.8 software from Oxford Instruments, supplied by the UCLA Broad Center of Regenerative Medicine & Stem Cell Research Microscopy Core. To ensure consistent acquisition of data across each image obtained, batch settings were applied to the entirety of the images. Under the batch settings, separate 3D renderings of channel-specific surfaces were created for each of the 4 channels (each channel corresponding to specific wavelengths of histological stains for visualization) and then applied to all the images. To obtain specific measurements for the distance of the pericytes from the border of the infarct region, the "object-object statistics" setting needed to be activated. Data on the cellular counts, positions, morphologies, volumes, areas, and intensities were recorded. Manual measurements from the pericytes to the infarct border could also be obtained using this software.

To mark the infarct border, an innovative method was utilized by initially outlining the infarct region within Adobe Illustrator with the Brush tool, saving the file as an .svg file, uploading that to an online 3D rendering website to then be exported as an .stl file, and then finally converted to a .wrl file through another online website. This process allowed for the generation of a 3D border that could be imported onto the Imaris software and measurements could be directly taken from this object.

Ratios (Heart Weight/Body Weight; Heart Weight/Tibia Length)

After sacrifice and perfusion with a saline IV (5 minutes) and formalin (15 minutes), the heart was excised, and all remaining fluid was gently squeezed out. To maintain consistency, all 4 chambers of the heart were present, and any excess fat or blood vessels were removed. The heart weight was then measured in milligrams and compared to the body weight measured prior to sacrifice. The tibia was harvested following the perfusion steps as well and measured with calipers from Fine Science Tools (30087-00).

Statistical Analysis

Data was expressed as mean +/- SEM for bar graph data presented and statistical analyses were performed using unpaired two-tailed Student's t-test when comparing two groups and One-Way ANOVA when comparing multiple groups. All measurements in this paper were acquired from distinct biological samples and no samples were measured repeatedly. To characterize the pericyte morphology for the preliminary data, an ordinary one-way ANOVA with multiple comparisons was utilized. In determining the pericyte density at various distances into the infarct, an unpaired two-tailed T-test was used. To analyze the echocardiogram data, two-way

ANOVA tests with multiple comparisons were used. Bar graph data analysis was performed using Graph Pad Prism 8 (Version 8.4.2). A value of $p<0.05$ was considered statistically significant.

RESULTS

Cspg4 lineage traces cardiac pericytes

As previously mentioned, CSPG4 was used as a marker for pericytes due to its predominant expression within these cells (Alex & Frangogiannis, 2019; Lee et al., 2019). To visualize and track pericytes over time, mice with a Cre-mediated CSPG4 background were crossed with mice in the Rosa26 Ai9$^{tdT/+}$ background to produce CSPG4$^{CreERT2/+}$;Rosa26 Ai9$^{tdT/+}$ mice whose pericytes would autofluoresce tdTomato (555nm) when exposed to tamoxifen **(Fig. 1A)**. Following 7 consecutive intraperitoneal tamoxifen injections, spaced 24 hours apart, the mice were subjected to MI for 5-, 7-, 10-, 14-, and 28-days **(Fig. 1B)**. These time points were chosen to study pericyte behavior during the inflammatory, proliferative, and maturation stages of the cardiac tissue post-ischemic-injury **(Fig. 1B)** (Pomara et al., 2015). We confirmed that our CSPG4$^{CreERT2/+}$; Rosa26 Ai9$^{tdTomato/+}$ mouse models expressed tdTomato exclusively in pericytes following tamoxifen administration **(Fig. 1C)**. For this study, we specifically focused on the peri-infarct region, composed of both healthy and damaged tissue, to study pericyte migration, morphology, and proliferation **(Fig. 1C)**.

Pericytes reach peak migration distances of greater than 45µm at 7dMI

In collaboration with Dr. Reza Ardehali's laboratory to measure pericyte migration into the infarct, a separate cohort of CSPG4$^{CreERT2/+}$; Rosa26 Ai9$^{tdT/+}$ mice were subjected to tamoxifen injections and subjected to MI for 2-, 4-, 7-, and 14-days. Over the MI time course, we observed that the pericytes migrated away from the microvasculature in the surrounding tissue and into the infarcted region **(Fig. 2A)**. To measure the distance of pericyte migration into the infarct, the shortest distance of pericytes within the infarcted tissue was measured to the

border zone using Imaris v9.8 **(Fig. 2G)**. Unfortunately, the total distance traveled by the pericytes prior to reaching the infarct could not be determined due to the inability to live-image pericytes. Quantification of the IHC images from **Fig. 2A** indicated that approximately 80-85% of pericytes were located within 0-45μm of the infarct border at the 2- and 4-day post-injury (2dMI, 4dMI) time points and then decreased to approximately 50-70% at the 7dMI and 14dMI time points respectively **(Fig. 2B)**. A significant increase in the pericytes found at a distance of greater than 45μm into the infarct were observed at the 7dMI and 14dMI time points **(Fig. 2B)**.

Pericytes increase in size at 7dMI and decrease in sphericity starting at 2dMI

Using the same cohort to study pericyte migration, data on pericyte volume, area, and sphericity were collected and analyzed using 3D rendering technology on Imaris v9.8 **(Fig. 2H)**. Pericytes showed increased cell volume and area at 7dMI and 14dMI as compared to pericytes observed in Sham controls **(Fig. 2C-D)**. Comparison of the Sham, 2dMI, and 4dMI time points to the 7dMI and 14dMI time points indicate a statistically significant increase in both pericyte volume and area **(Fig. 2D)**. Pericyte sphericity decreased between the 2dMI and 14dMI time points consistent with increases in cell size. **(Fig. 2D)**. Together, this data suggests that the pericytes increase in size following a MI while also decreasing in sphericity.

Pericyte proliferation peaks at 14-days post-injury

To study pericyte proliferation, CSPG4$^{CreERT2/+}$; Rosa26 Ai9$^{tdT/+}$ mice were administered tamoxifen and subjected to MI for of 5-, 7-, 10-, 14-, and 28-days. Following MI, Ki67 expression increased at the 5dMI, 7dMI, and 14dMI time points in comparison with the Sham

and 28dMI time points **(Fig. 3)**. We also measured an increase in the number of pericytes visualized at the 14dMI time point **(Fig. 3 & Fig. 4A)**. To quantify the cellular proliferation occurring at each time point, 3D rendering analysis was used in Imaris v9.8 to determine Ki67-expressing cell distribution **(Fig. 4A)**. In comparison to other cell types, pericytes had the least expression of Ki67, followed by endothelial cells, and then non-pericyte/non-endothelial cell/non-cardiomyocyte cells (non-PC/EC/CM) **(Fig. 4A)**. Cardiomyocytes were ruled out as proliferating cells due to their post-mitotic state and limited ability to regenerate, thereby leaving immune cells and fibroblasts as the cells within the non-PC/EC/CM population (Fu et al., 2018; Payan et al., 2020; Xin et al., 2013). Within the non-PC/EC/CM cell population, there was a statistically significant increase in the average number of cells undergoing proliferation at the 5dMI time point when compared with the Sham and 28dMI time points **(Fig. 4A)**. The percent proliferation of each cell type was calculated at each of the respective time points **(Fig. 4B-D)**. When normalized to each cell type, approximately 28% of pericytes were undergoing proliferation at 14dMI **(Fig. 4B)**. The percent proliferation amongst the endothelial cells over the MI time course remained relatively constant between 7-10% **(Fig. 4C)**. A sharp increase in the percentage of non-PC/EC/CM cells undergoing proliferation at the 5dMI time point in comparison to the other time points was observed as well **(Fig. 4D)**. These results were consistent with the findings in Fu et al., 2018, which demonstrated that fibroblasts underwent proliferation within 3-5 days post-injury (Fu et al., 2018). Together, these findings suggest that pericytes will undergo peak proliferation around the 14dMI time point whereas the non-PC/EC/CM cells will undergo peak proliferation at the 5dMI time point for this particular MI time course.

To measure the impacts of MI on cardiac function, physiological data from our 5-, 7-, 10-, 14-, and 28-day CSPG4$^{CreERT2/+}$; Rosa26 Ai9$^{tdT/+}$ mouse cohort were collected as well **(Fig. 4E)**. Compensatory hypertrophy in the heart was measured using the ratios between heart weight and body weight (HW/BW) as well as the ratio between heart weight and tibia length (HW/TL) **(Fig. 4E)** (Rubin et al., 1983). In comparison to Sham, there was a general increase in HW/BW and HW/TL ratios, thereby indicating increased hypertrophy in the animal hearts and the presence of a MI **(Fig. 4E)**. Despite the HW/BW and HW/TL ratios of the 14dMI mice and one 7dMI mouse being similar to the Sham mice ratio values, we did observe MIs in all of the mice subjected to LAD ligation. Unfortunately, no data can be presented on the 10dMI mice as none survived the LAD ligation surgery **(Fig. 4F)**.

P53 deletion in cardiac pericytes does not alter cardiac function

To further characterize pericyte roles and functions following an acute ischemic injury, the cell cycle regulator, p53, was knocked out within pericytes **(Fig. 5A)** (Levine, 1997). Due to the timing limitation for this thesis, the proposed model organism, CSPG4$^{CreERT2/+}$;R26$^{tdT/+}$;p53$^{flox/flox}$ was unable to be used and only CSPG4$^{CreERT2/+}$;p53$^{flox/flox}$ mice were used for conducting baseline measurements **(Fig. 5A)**. Due to the unknown impact of completely knocking out p53 in pericytes, p53$^{flox/+}$ and p53$^{+/+}$ mice were also included to measure any phenotypic differences. To measure cardiac function, echocardiograms were performed at 2-week intervals up to 6-weeks post-TAM administration. There was a statistically significant difference in the systolic volume and ejection fraction between the p53$^{flox/flox}$ and p53$^{flox/+}$ mice at the 4-week time point **(Fig. 5B-C)**. However, in the context of the 6-week period, the overall systolic volume and ejection fraction showed little difference **(Fig. 5B-C)**.

Together, this data suggests that the deletion of p53 from the cardiac pericyte lineage does not alter the cardiac physiology under homeostatic conditions.

DISCUSSION

Based on the results, our hypothesis that pericytes would undergo increased proliferation and migration following the generation of the inflammatory or angiogenic cues released from the damaged myocardial and vascular tissue was partially supported. As illustrated in **Fig. 2A-F**, pericyte migration did increase in response to cardiac injury followed by an increase in cell size over time. In conjunction with the results illustrated in **Fig. 3** and **Fig. 4A-B**, the increase in reported pericyte size may have been the result of pericyte proliferation occurring at its peak during the 14dMI time point. This data suggests that following an ischemic cardiac injury, pericytes will initially detach from the microvasculature, retract their finger-like projections to adopt a more spherical shape, and then migrate into the infarct where these cells will undergo increases in cell size and cellular proliferation. Together, these results suggest that the pericytes do not adopt a pro-angiogenic role once they enter the infarct, but instead assume a pro-fibrotic role when the heart is subjected to ischemic injury. Therefore, the results partially support the hypothesis that once pericytes enter the infarct, they will aid in the process of interstitial tissue reformation through the secretion of extracellular matrix factors and pro-inflammatory cell recruitment to mediate fibrotic remodeling and vascular recovery. However, further investigation needs to be conducted to test this theory.

Considering the results found with respect to pericyte migration, morphology, proliferation, and roles in fibrosis, we suspect that the previous hypothesis, that the functional KO out p53 within pericytes would result in rapid proliferation and increased angiogenesis, would be partially supported. We suspect that the pericytes will undergo increased proliferation due to the loss of the cell cycle regulator; however, we also suspect that the pericytes will not

increase angiogenesis but will instead increase the expansion of the fibrotic scar tissue. We also suspect that in conjunction with the KO of p53 in the pericytes, that the expansion of the fibrotic scar tissue will increase at an exponentially faster rate. However, further investigation also needs to be conducted to determine how the pericytes with the functional KO of p53 will react when subjected to ischemic conditions.

We are excited to present this data as it provides new insights on pericyte behavior and function following an ischemic injury. While further investigation is needed to characterize the cardiac pericytes, this study provides new information on pericyte proliferation and migration that has not yet been demonstrated.

FUTURE DIRECTIONS

To further elucidate the proliferation of pericytes within and around the infarct, we are currently breeding mice in the CSPG4$^{CreERT2/+}$; Rosa26 Ai9$^{tdT/+}$ background to experiment on 14dMI and other time points (such as 3dMI, 10dMI, and 21dMI) to provide a more comprehensive understanding of pericyte behavior after injury. We are also continuing to breed mice for Specific Aim 2 of the CSPG4$^{CreERT2/+}$; p53$^{flox/flox}$ background to determine the impact of knocking out the p53 cell-cycle regulator in pericytes on cardiac function both with and without injury as measured in echocardiograms. The results for Specific Aim 2 will also help characterize the roles that pericytes play in scar formation and/or vascular remodeling. We also plan on further characterizing the pericytes by performing single cell RNA-sequencing on the pericytes to determine if there are genetic subpopulations within pericytes seen in the heart. These transcripts will be analyzed to determine if the pericytes assume various roles under different conditions.

Another direction that is of interest to us is the mechanism by which the pericytes detach from the microvasculature as this has not been previously discovered. Certain extracellular matrix proteins such as MMP14 have been thought to play a role in adhering pericytes to the blood vessels, however, this would require further experimentation to determine. Furthermore, we are interested in studying how the pericytes migrate as well. It is currently unknown whether the pericytes migrate based off chemical signals, molecular signals, or electrical signals. Certain molecular or chemical signals in the blood could interact with chemoreceptors on the cell-surface of the pericytes indicating a loss in vascular integrity that could induce pericyte disassociation from the vasculature and migration towards the source. By understanding the molecular and

cellular mechanisms by which pericytes detach and migrate, in conjunction with the migration, morphology, and proliferation data presented in this paper, this information could allow us to better characterize pericyte roles and behaviors in response to an acute ischemic injury.

LIMITATIONS

In studying pericyte migration and proliferation, the total number of mice that were able to participate in the experiment were limited due to the breeding schedule and the generation of mice that were specific to the genetic background desired. This was also compounded by the survival rate of the mice following MI surgery as seen in the 10dMI (0% survival), 14dMI (66.67% survival), and 28dMI (60% survival) **(Fig. 4F)**. Furthermore, the breeding schedules and postnatal survival for creating a triple-transgenic mouse for specific aim 2 limited our ability to produce a large cohort of animals for experimentation.

FIGURES

Figure 1

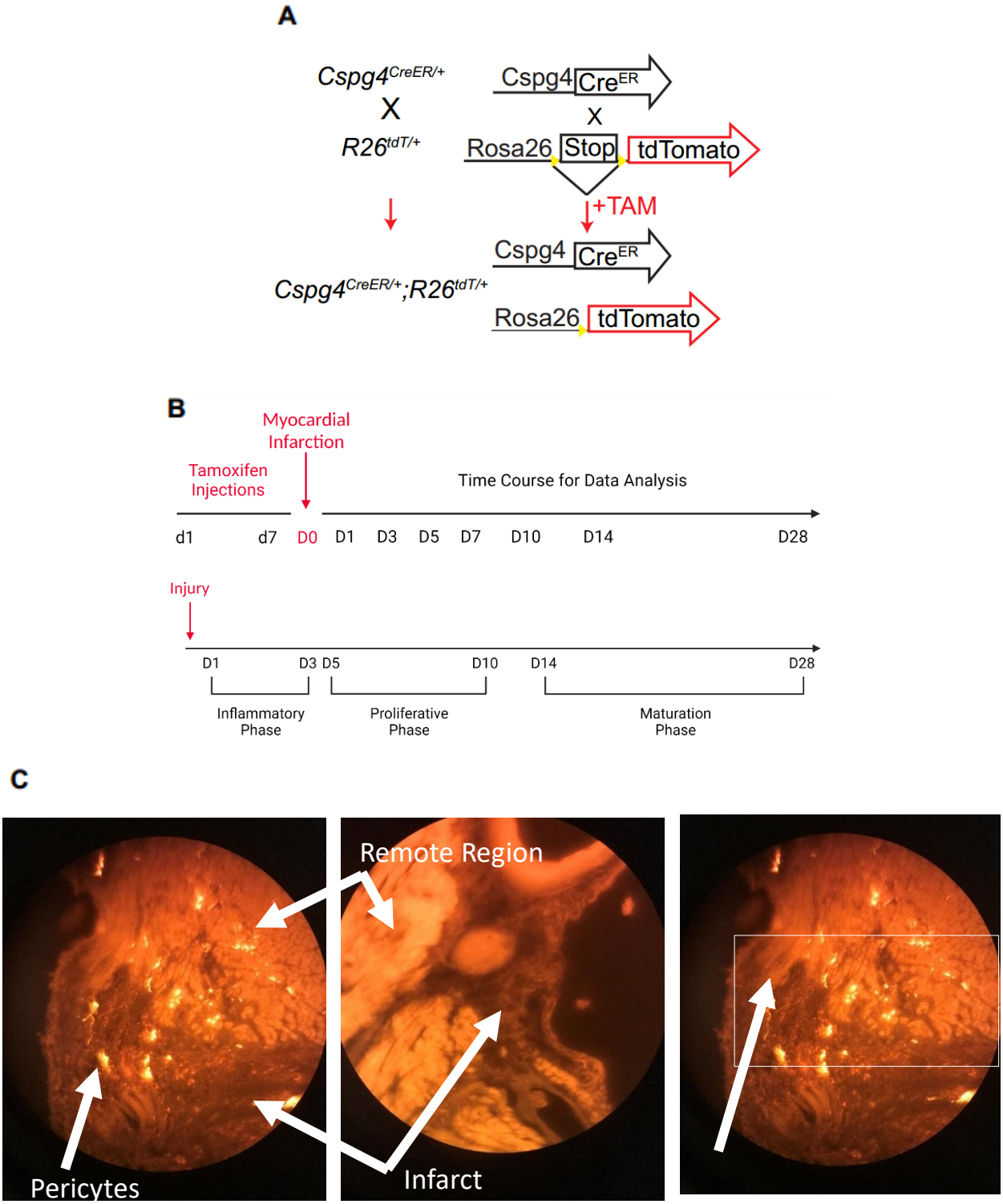

Figure 1. Specific Aim 1 Experimental Set Up. **(A)** Mice with a Cre-driven promoter in the *Cspg4* gene were crossed to *Rosa26*$^{tdT/+}$ mice and the progeny were administered tamoxifen to induce lineage-tracing pericyte fluorescence. **(B)** Mice were subjected to 7 days of intraperitoneal tamoxifen injections followed by MI surgery and kept until the following time points (5dMI, 7dMI, 10dMI, 14dMI, and 28dMI). These time points were chosen based on the cardiac-specific-repair timeline discussed in Turillazzi et al., 2015. **(C)** Pericyte migration was measured at the peri-infarct region and only CSPG4$^{CreERT2/+}$;Rosa26 Ai9$^{tdT/+}$ mice were used. The middle image demonstrates lack of pericyte fluorescence. Images were taken through the ocular lens on a Zeiss LSM 700 Confocal Microscope on a 20x objective lens. Remote regions are composed of healthy cardiac tissue. Infarcted regions are composed of dead/dying cardiac tissue. The border zone designates the separation between the healthy and necrotic cardiac tissue.

Figure 2

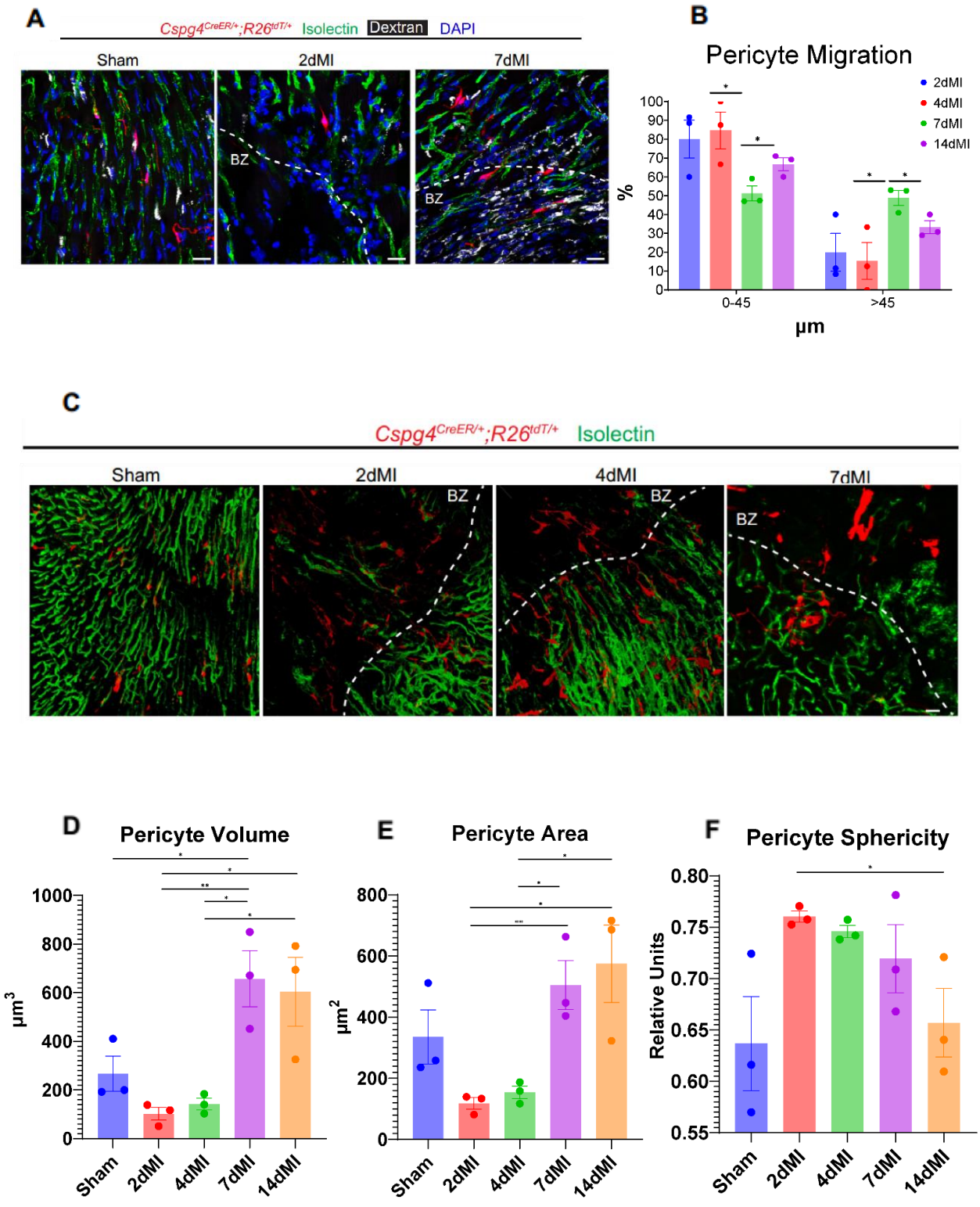
A
Cspg4CreER/+;R26tdT/+ Isolectin Dextran DAPI
Sham
2dMI
7dMI
BZ
BZ
B
Pericyte Migration
2dMI
4dMI
7dMI
14dMI
%
0-45
>45
µm
C
Cspg4CreER/+;R26tdT/+ Isolectin
Sham
2dMI
4dMI
7dMI
BZ
BZ
BZ
D
Pericyte Volume
µm3
E
Pericyte Area
µm2
F
Pericyte Sphericity
Relative Units
Sham
2dMI
4dMI
7dMI
14dMI

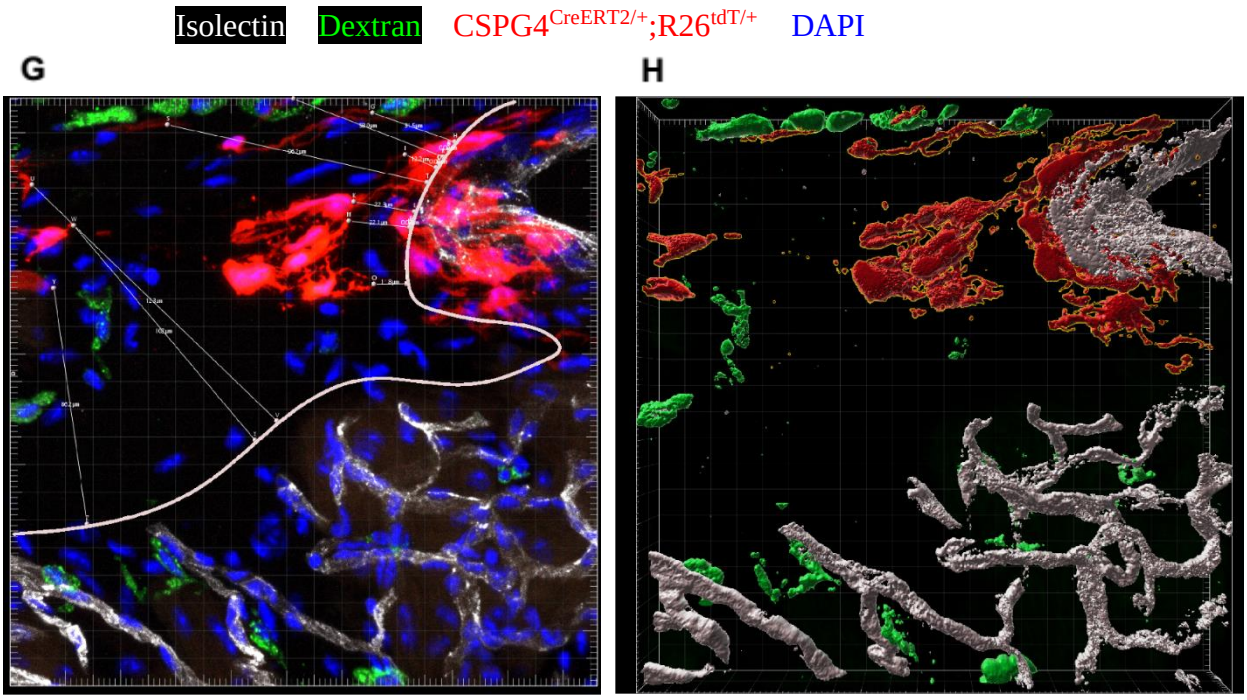

Figure 2. Pericyte Migration and Morphology. **(A)** Confocal microscopy images of the peri-infarct region of immunohistochemistry-stained cardiac tissue at the Sham, 2dMI, and 7dMI time points with the border zone (BZ) denoted by the dashed line. Intact vasculature marked by the Isolectin (green) is visualized within the heathy tissue and absent in the necrotic tissue. Biotinylated-Dextran (white; indicating leaky vasculature) and Isolectin were administered to the mice on the day of isolation. Pericytes (red) are visualized in the peri-infarct region. **(B)** Quantification of the percentage of pericyte migration into the infarcted region with statistical significance between the 4dMI to 7dMI and 7dMI to 14dMI measured distances. **(C)** Pericyte morphology increased in size over time following acute ischemic injury. **(D-F)** Quantification of pericyte morphology changes over time using Imaris v9.8. Pericyte volume and area increased from the 2dMI and 4dMI time points to the 7dMI and 14dMI time points. Pericytes decreased in sphericity over time and was statistically significant between 2dMI to 14dMI comparison. **(G)** Measurement procedure of the shortest distance to the infarct border using Imaris v9.8 using

imported image-specific border zones. Isolectin (white) and Biotinylated-Dextran (green) were administered the day of isolation. **(H)** 3D rendering of the peri-infarct region using Imaris v9.8 of G. Scale bar: 20μm. *$p<0.05$, **$p<0.01$.

Figure 3

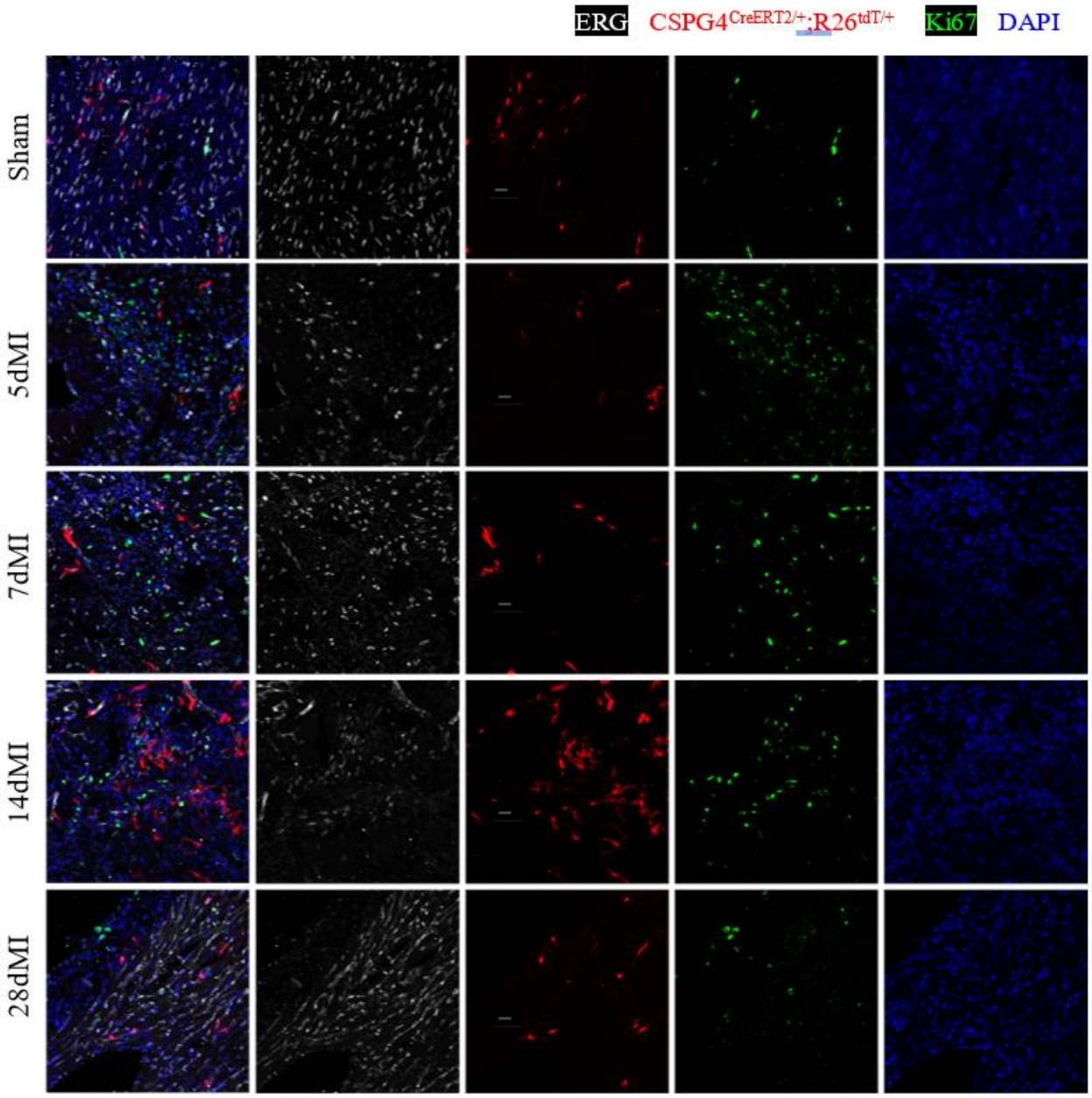
ERG
CSPG4CreERT2/+;R26tdT/+
Ki67
DAPI
Sham
5dMI
7dMI
14dMI
28dMI

Figure 3. Pericyte Proliferation Time Course. Individual channel and merged confocal images of cardiac tissue in the left ventricle over time. Ki67 antibody (green) was used to label proliferating cells within the peri-infarct region for the MI time course and proliferating cells in the left ventricle for Sham. There was an increase in the number of cells proliferating at the 5dMI time point compared to the other time points. ERG (white) stained the endothelial cells in the peri-infarct region. Isolectin was injected via tail vein injection on the day of isolation for all mice, but only successful injections can be seen at the 14dMI and 28dMI images. Increased pericyte (red) presence can be seen at the 14dMI time point. Scale bar: 20μm.

Figure 4

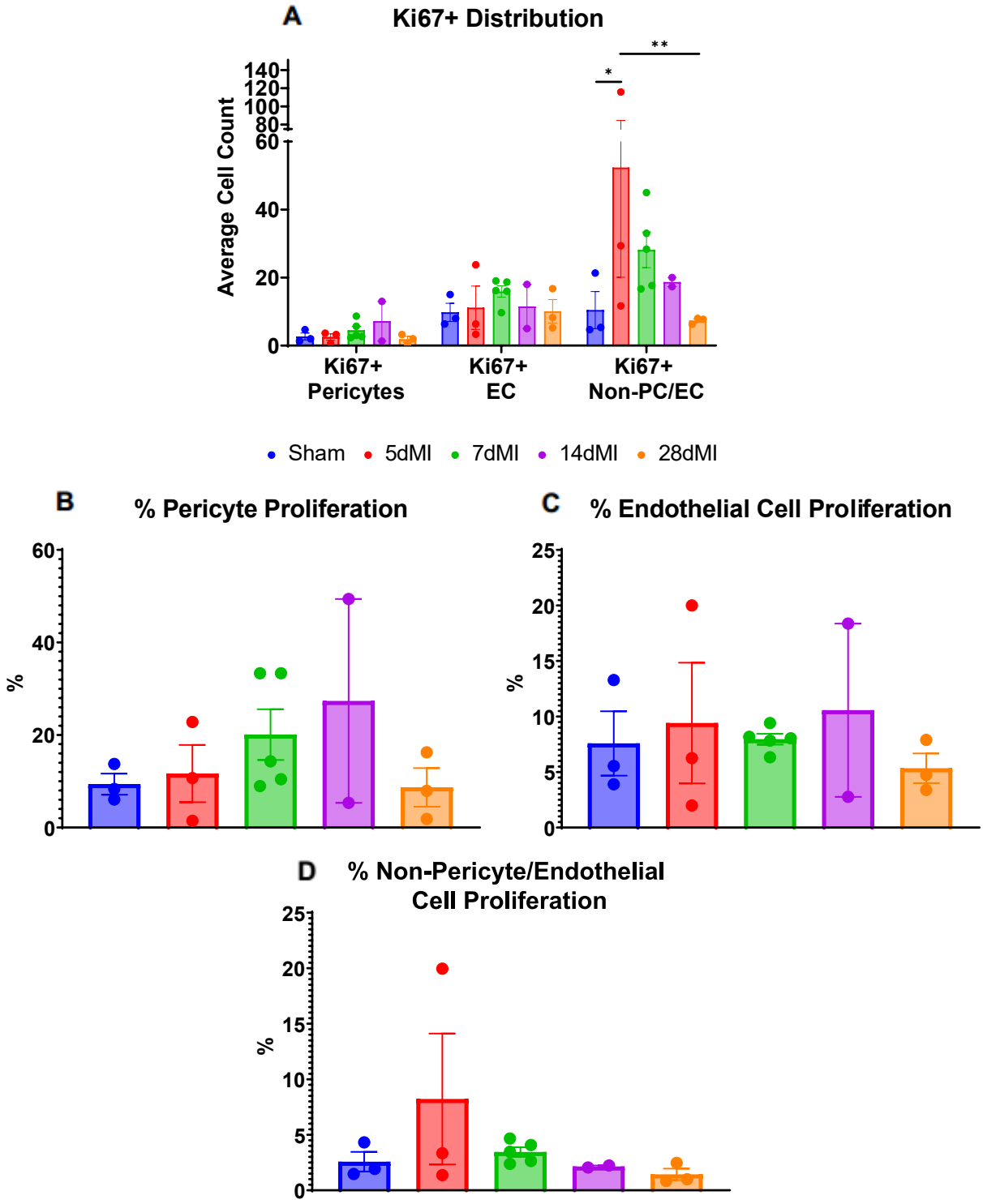
A
Ki67+ Distribution
Average Cell Count
140
120
100
80
60
40
20
0
*
**
Ki67+ Pericytes
Ki67+ EC
Ki67+ Non-PC/EC
Sham
5dMI
7dMI
14dMI
28dMI
B
% Pericyte Proliferation
%
60
40
20
0
C
% Endothelial Cell Proliferation
%
25
20
15
10
5
0
D
% Non-Pericyte/Endothelial Cell Proliferation
%
25
20
15
10
5
0

E

Genotype	Sex	Surgery	HW	BW	TL	HW/BW	HW/TL
$CSPG4^{CreERT2/+}$;$Ai9^{flox/flox}$; $Col1a1GFP^{+}$	F	Sham*	86.1	21.33	18.45	4.04	4.67
$CSPG4^{CreERT2/+}$;$Ai9^{flox/flox}$; $Col1a1GFP^{+}$	M	Sham*	127.1	26.52	17.22	4.79	7.38
$CSPG4^{CreERT2/+}$;$Ai9^{flox/+}$; $Col1a1GFP^{+}$	M	Sham*	124.1	28.32	17.12	4.38	7.25
CSPG4^{CreERT2};Ai9/+	M	5dMI	179.1	23.38	17.34	7.66	10.33
CSPG4^{CreERT2};Ai9/+	M	5dMI	146.6	26.36	17.71	5.56	8.28
CSPG4^{CreERT2};Ai9/+	M	5dMI	149	25.41	17.61	5.86	8.46
CSPG4^{CreERT2};Ai9/+	F	7dMI	161.2	19.75	17.48	8.16	9.22
CSPG4^{CreERT2};Ai9/+	F	7dMI	120.4	19.61	17.62	6.14	6.83
CSPG4^{CreERT2};Ai9/+	F	7dMI	93.4	20.90	18.75	4.47	4.98
CSPG4^{CreERT2};Ai9/+	F	7dMI	133.4	19.97	17.91	6.68	7.45
CSPG4^{CreERT2};Ai9/+	F	7dMI	124.1	21.50	17.83	5.77	6.96
CSPG4^{CreERT2};Ai9/+	M	14dMI	104.7	23.38	23.86	4.48	4.39
CSPG4^{CreERT2};Ai9/+	M	14dMI	111.0	23.78	21.68	4.67	5.12
CSPG4^{CreERT2};Ai9/+	F	28dMI	115.4	20.25	18.99	5.70	6.08
CSPG4^{CreERT2};Ai9/+	F	28dMI	128.6	20.24	17.85	6.35	7.20
CSPG4^{CreERT2};Ai9/+	F	28dMI	146.7	19.03	18.50	7.71	7.93

F

Surgery	Number of Mice in Cohort	Number of Mice Survived	% MI Survival
Sham*	3	3	100
5dMI	3	3	100
7dMI	5	5	100
10dMI	4	0	0
14dMI	3	2	66.67
28dMI	5	3	60

Figure 4. Proliferating Cell Type Quantification. Quantification of proliferating cells was conducted on Imaris v9.8. **(A)** Total counts of each cell type (pericytes, endothelial cells, and non-pericytes/non-endothelial cells/non-cardiomyocytes) were averaged for each time point. A

statistically significant increase from Sham to5dMI was noticed in the non-pericytes/non-endothelial cells/non-cardiomyocyte cell population. There was also a statistically significant decrease in the non-pericytes/non-endothelial cells/non-cardiomyocyte cells from the 5dMI to the 28dMI time points. No statistically significant differences were determined between the number of endothelial cells or pericytes in the average cell counts. **(B-D)** Percent cell-type-specific proliferation by time point was calculated by the following: $\frac{Average\ Number\ of\ Specific\ Proliferating\ Cell\ Type\ Cells}{Total\ Number\ of\ Cell\ Type\ Specific\ Cells} \times 100\%$. No statistically significant differences were noted in the proliferating cell-type percentages for the pericytes, endothelial cells, or non-pericytes/non-endothelial cells/non-cardiomyocytes. **(E)** Table of physiological measurements taken on the day of tissue isolation. Heart weight/body weight and heart weight/tibia length were measured to monitor compensatory hypertrophy. **(F)** Table of mouse survival following the MI surgeries. Sham* mice physiological data were taken from a separate cohort of genetically similar mice (with an extra lineage tracer for Collagen 1A1) for comparison. *$p<0.05$, **$p<0.01$.

Figure 5

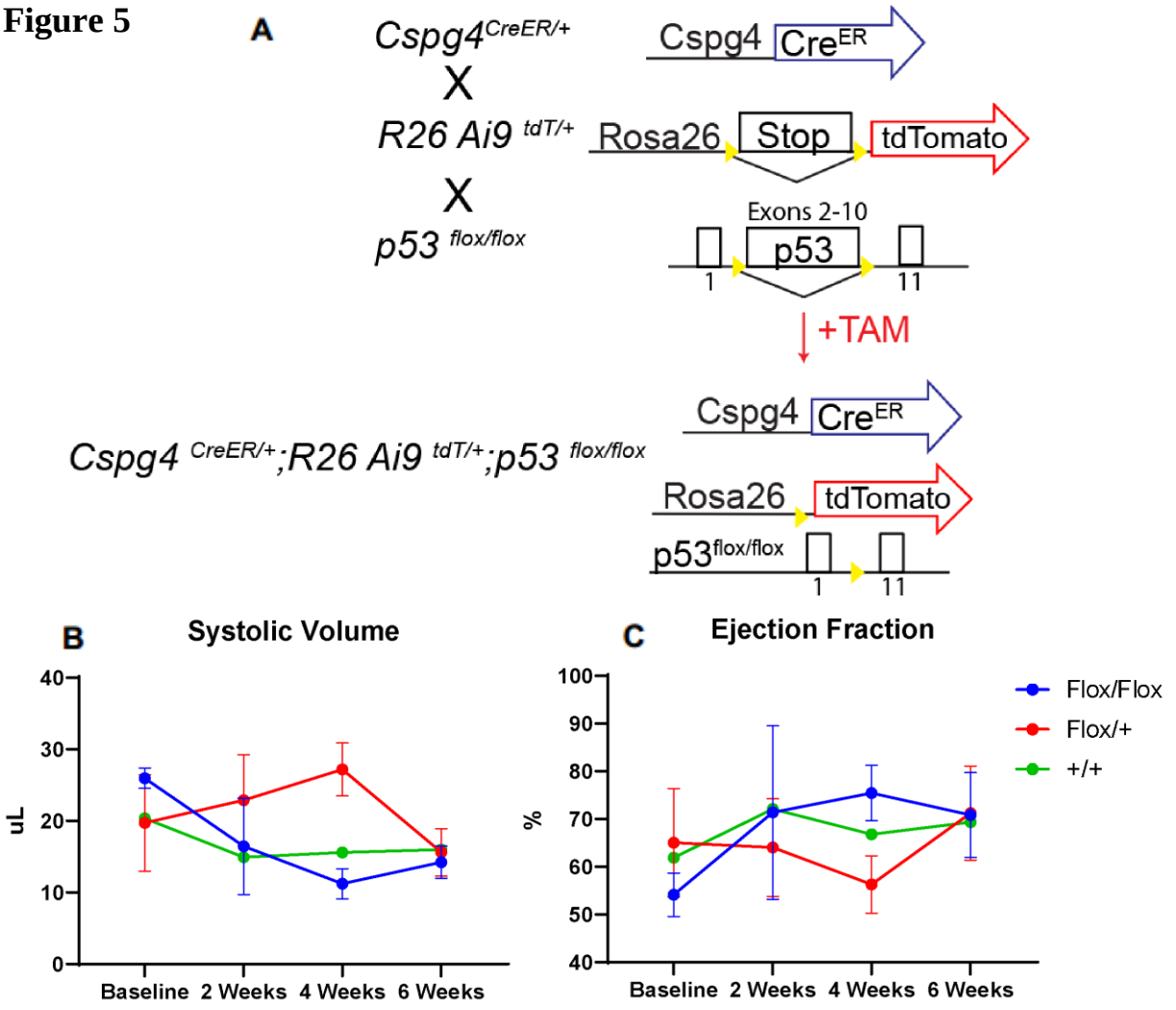

D

Genotype	Sex	Surgery	HW	BW	TL	HW/BW	HW/TL
CSPG4$^{CreERT2/+}$; p53$^{flox/flox}$	M	Sham	143.2	29.00	17.98	4.94	7.96
CSPG4$^{CreERT2/+}$; p53$^{flox/flox}$	M	Sham	130.6	27.00	17.83	4.84	7.32
CSPG4$^{CreERT2/+}$; p53$^{flox/flox}$	F	Sham	128.3	22.27	18.06	5.76	7.10
CSPG4$^{CreERT2/+}$; p53$^{flox/flox}$	F	Sham	131.4	21.66	19.30	6.07	6.81
CSPG4$^{CreERT2/+}$; p53$^{flox/flox}$	F	Sham	123.7	22.24	17.98	5.56	6.88
CSPG4$^{CreERT2/+}$; p53$^{flox/+}$	M	Sham	169.3	28.80	17.69	5.88	9.57
CSPG4$^{CreERT2/+}$; p53$^{flox/+}$	M	Sham	150.4	27.30	18.4	5.51	8.17
CSPG4$^{CreERT2/+}$; p53$^{flox/+}$	F	Sham	138.4	22.85	18.61	6.06	7.44
CSPG4$^{CreERT2/+}$; p53$^{+/+}$	F	Sham	116.4	21.70	18.16	5.36	6.41

Figure 5. Specific Aim 2 Experimental Set Up and Baseline Measurements. **(A)** Experimental set up for Specific Aim 2. The model organism was a CSPG4$^{CreERT2/+}$;Rosa26 Ai9$^{tdT/+}$;p53$^{flox/flox}$ mouse with a fluorescent lineage tracer to label pericytes while also knocking out the *p53* cell cycle regulator gene. Sham mice were of the CSPG4$^{CreERT2/+}$;p53$^{flox/flox\ or\ flox/+\ or\ +/+}$ background. **(B-C)** Echocardiogram data for CSPG4$^{CreERT2/+}$;p53$^{flox/flox}$ mice without injury were collected for 6 weeks. No phenotypes were noticed between the p53 KO, p53 partial KO, and p53 WT. At the 4-week time point, there was a statistically significant difference between the p53 partial KO and the p53 KO in both the systolic volume and ejection fraction. **(D)** Table of the physiological data collected on the day of tissue isolation. HW/BW and HW/TL ratios were calculated to monitor compensatory hypertrophy. *$p<0.05$.

Supplementary Figure 1

Supplementary Figure 1. Echocardiography Procedures. Probe placement for the specific heart measurements. Long axis and short axis probe placement will be perpendicular to the mouse. 4-Chamber view will require the probe to be placed at a 45° angle to the body. Long axis view ensures that the probe is placed in the correct area. The probe is then turned clockwise by 90° to view the short axis. Short axis views can be measured to determine cardiac function. 4-Chamber views can measure the systolic and diastolic function of the heart by using the pulse wave doppler and tissue wave doppler settings.

Supplementary Figure 2

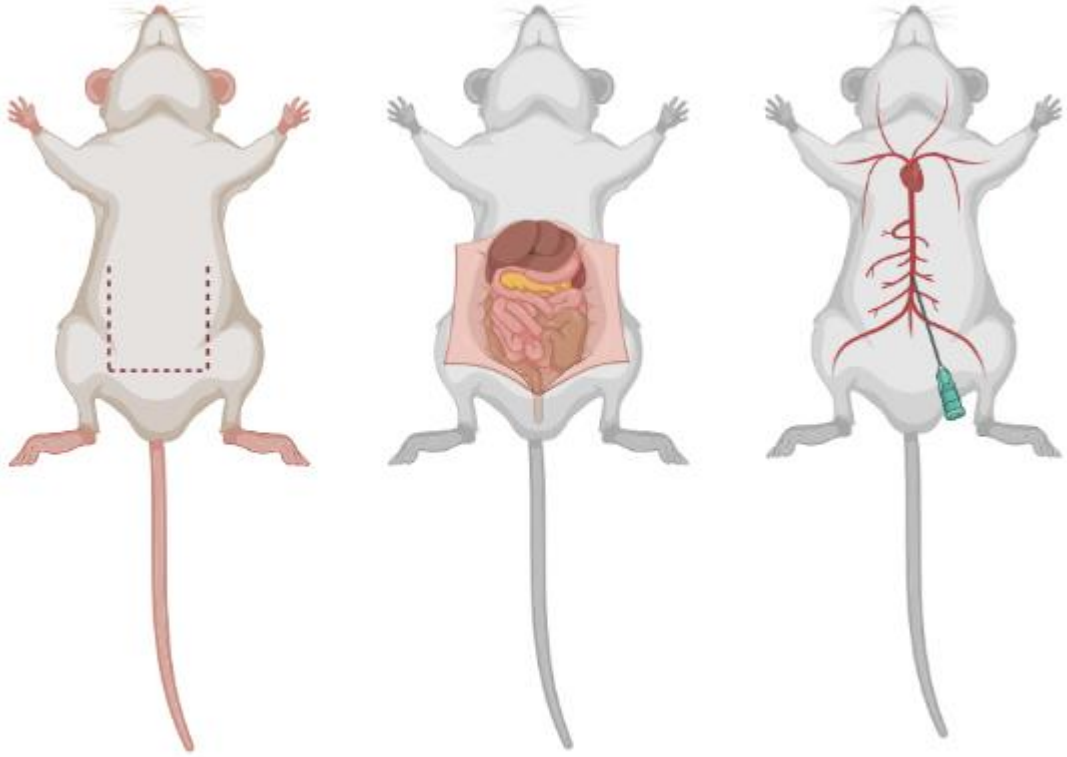

Supplementary Figure 2. Tissue Perfusion and Procurement Procedures. Following ketamine intraperitoneal injections, the mice are placed with their ventral side exposed. The skin is cut at the dotted lines and the internal organs will be exposed. The internal organs should be gently displaced using a cotton-tipped applicator to expose the IVC and AA. Once the distal portion of the AA and IVC are sutured and the rostral portion of the IVC and AA are clamped, a small incision will be made in the AA allowing a cannula to be placed into the AA. The clamp will be placed over the cannula in the AA to maintain cannula position and retro-perfusion will begin. Potassium chloride will be used to stop the heart. Tissue procurement and isolation will occur after 5 minutes of hypertonic saline solution and 15 minutes of formalin solution is administered.

Table S1. Experimental Staining Set Up

Stain of Interest	Primary Antibody Stains	Secondary Antibody Stains	Spectrum Emissions
BrdU	Rat BrdU Rabbit ERG	DAPI – 405nm DαRat – 488nm DαRabbit – 647nm	405nm – DAPI 488nm – BrdU 555nm – tdTomato 647nm – ERG
Ki-67	Rat Ki-67 Rabbit ERG	DAPI – 405nm DαRat – 488nm DαRabbit – 647nm	405nm – DAPI 488nm – Ki-67 555nm – tdTomato 647nm – ERG
PCNA	Goat PCNA Rabbit ERG	DAPI – 405nm DαGoat – 488nm DαRabbit – 647nm	405nm – DAPI 488nm – PCNA 555nm – tdTomato 647nm – ERG

Table S2. List of Primary Antibodies

Company	Catalog Number	Host	Target	Name
Abcam	Ab6326	Rat	Unspecified	Rat monoclonal [BU1/75 (ICR1)] to BrdU - Proliferation Marker
Abcam	Ab92513	Rabbit	Unspecified	Rabbit monoclonal antibody to ERG
Abcam	Ab115555	Goat	Human, Mouse, Rat, Horse	Anti-ERG Antibody
LS Bio	LS-B14132-50	Goat	Human, Mouse, Rat, Bovine, Dog, Guinea pig, Hamster, Horse, Pig, Rabbit, Chicken	Goat anti-Human PCNA Antibody
ThermoFisher Scientific	14-5698-82	Rat	Dog, Cynomolgus monkey, Human, Mouse, Non-human primate, Rat	Ki-67 Monoclonal Antibody (SolA15), eBioscience
ThermoFisher Scientific	13-4100	Mouse	Mouse, Human, Rat	p53 Monoclonal Antibody
Millipore Sigma	Ab5320	Rabbit	Mouse, Rat, Human, Monkey	Anti-NG2 Chondroitin Sulfate Proteoglycan

Table S3. List of Secondary Antibodies

Company	Catalog Number	Host	Target	Name
Jackson ImmunoResearch	712-545-153	Donkey	Rat	488-AffiniPure Donkey Anti-Rat IgG (1.5mg/mL)
Fisher Scientific	I32450	Unspecified	Unspecified	Isolectin GS-IB4 647
Jackson ImmunoResearch	705-545-147	Donkey	Goat	Alexa Fluor 488-conjugated AffiniPure Donkey Anti-Goat IgG (1.5mg/mL)
Jackson ImmunoResearch	711-605-152	Donkey	Rabbit	Alexa Fluor 647-conjugated AffiniPure Donkey Anti-Rabbit IgG (1.5mg/mL)
Jackson ImmunoResearch	715-605-150	Donkey	Mouse	Alexa Fluor 647 conjugated (1.5mg/mL)
Jackson ImmunoResearch	711-065-152	Donkey	Rabbit	Biotin-SP-conjugated Donkey anti-Rabbit (1mg/mL)
Thermo Fisher Scientific	S21381	Unspecified	Unspecified	Streptavidin Alexa Fluor 555 conjugate (2mg/mL)
BD Biosciences	BD 564907	Unspecified	Nuclei	DAPI (1mg/mL)

BIBLIOGRAPHY

1. Alex, L., & Frangogiannis, N. G. (2019). Pericytes in the infarcted heart. Vascular Biology, 1(1), H23-H31. https://doi.org/10.1530/vb-19-0007
2. Armulik, A., Abramsson, A., & Betsholtz, C. (2005). Endothelial/Pericyte Interactions. Circulation Research, 97(6), 512-523. https://doi.org/10.1161/01.res.0000182903.16652.d7
3. Attwell, D., Mishra, A., Hall, C. N., O'Farrell, F. M., & Dalkara, T. (2016). What is a pericyte? Journal of Cerebral Blood Flow & Metabolism, 36(2), 451-455. https://doi.org/10.1177/0271678x15610340
4. Avolio, E., & Madeddu, P. (2016). Discovering cardiac pericyte biology: From physiopathological mechanisms to potential therapeutic applications in ischemic heart disease. Vascular Pharmacology, 86, 53-63. https://doi.org/10.1016/j.vph.2016.05.009
5. Bahit, M. C., Kochar, A., & Granger, C. B. (2018). Post-Myocardial Infarction Heart Failure. JACC Heart Fail, 6(3), 179-186. https://doi.org/10.1016/j.jchf.2017.09.015
6. Beltrami, A. P., & Madeddu, P. (2018). Pericytes and cardiac stem cells: Common features and peculiarities. Pharmacological Research, 127, 101-109. https://doi.org/10.1016/j.phrs.2017.05.023
7. Bergers, G., & Song, S. (2005). The role of pericytes in blood-vessel formation and maintenance. Neuro-Oncology, 7(4), 452-464. https://doi.org/10.1215/s1152851705000232
8. Bersell, K., Arab, S., Haring, B., & Kühn, B. (2009). Neuregulin1/ErbB4 Signaling Induces Cardiomyocyte Proliferation and Repair of Heart Injury. Cell, 138(2), 257-270. https://doi.org/10.1016/j.cell.2009.04.060
9. Braile, M., Marcella, S., Cristinziano, L., Galdiero, M. R., Modestino, L., Ferrara, A. L., Varricchi, G., Marone, G., & Loffredo, S. (2020). VEGF-A in Cardiomyocytes and Heart

Diseases. International Journal of Molecular Sciences, 21(15), 5294. https://doi.org/10.3390/ijms21155294

10. Brown, L. S., Foster, C. G., Courtney, J.-M., King, N. E., Howells, D. W., & Sutherland, B. A. (2019). Pericytes and Neurovascular Function in the Healthy and Diseased Brain. Frontiers in cellular neuroscience., 13, 282. https://doi.org/10.3389/fncel.2019.00282
11. Cai, W., Liu, H., Zhao, J., Chen, L. Y., Chen, J., Lu, Z., & Hu, X. (2017). Pericytes in Brain Injury and Repair After Ischemic Stroke. Translational Stroke Research, 8(2), 107-121. https://doi.org/10.1007/s12975-016-0504-4
12. Chen, J., Luo, Y., Hui, H., Cai, T., Huang, H., Yang, F., Feng, J., Zhang, J., & Yan, X. (2017). CD146 coordinates brain endothelial cell–pericyte communication for blood–brain barrier development. Proceedings of the National Academy of Sciences, 114(36), E7622-E7631. https://doi.org/10.1073/pnas.1710848114
13. Chen, Q., Zhang, H., Liu, Y., Adams, S., Eilken, H., Stehling, M., Corada, M., Dejana, E., Zhou, B., & Adams, R. H. (2016). Endothelial cells are progenitors of cardiac pericytes and vascular smooth muscle cells. Nature Communications, 7(1), 12422. https://doi.org/10.1038/ncomms12422
14. D'Amore, P. A., & Sakurai, M. K. (2006). ANGIOGENESIS, ANGIOGENIC GROWTH FACTORS AND DEVELOPMENT FACTORS. Encyclopedia of respiratory medicine /, 110-115. https://doi.org/10.1016/B0-12-370879-6/00027-2
15. DeLisser, H. M. (2006). ADHESION, CELL–CELL | Vascular. Encyclopedia of respiratory medicine /, 29-37. https://doi.org/10.1016/B0-12-370879-6/00008-9
16. Devaux, Y., Bousquenaud, M., Rodius, S., Marie, P.-Y., Maskali, F., Zhang, L., Azuaje, F., & Wagner, D. R. (2011). Transforming growth factor β receptor 1 is a new candidate

prognostic biomarker after acute myocardial infarction. BMC Medical Genomics, 4(1), 83. https://doi.org/10.1186/1755-8794-4-83

17. Eilken, H. M., Diéguez-Hurtado, R., Schmidt, I., Nakayama, M., Jeong, H.-W., Arf, H., Adams, S., Ferrara, N., & Adams, R. H. (2017). Pericytes regulate VEGF-induced endothelial sprouting through VEGFR1. Nature Communications, 8(1). https://doi.org/10.1038/s41467-017-01738-3
18. Fernández-Klett, F., Offenhauser, N., Dirnagl, U., Priller, J., & Lindauer, U. (2010). Pericytes in capillaries are contractile in vivo, but arterioles mediate functional hyperemia in the mouse brain. Proceedings of the National Academy of Sciences, 107(51), 22290-22295. https://doi.org/10.1073/pnas.1011321108
19. Frangogiannis, N. G. (2012). Regulation of the Inflammatory Response in Cardiac Repair. Circulation Research, 110(1), 159-173. https://doi.org/10.1161/circresaha.111.243162
20. Frangogiannis, N. G. (2014). The inflammatory response in myocardial injury, repair, and remodelling. Nature Reviews Cardiology, 11(5), 255-265. https://doi.org/10.1038/nrcardio.2014.28
21. Frangogiannis, N. G. (2019). Cardiac fibrosis: Cell biological mechanisms, molecular pathways and therapeutic opportunities. Molecular Aspects of Medicine, 65, 70-99. https://doi.org/10.1016/j.mam.2018.07.001
22. Fu, X., Khalil, H., Kanisicak, O., Boyer, J. G., Vagnozzi, R. J., Maliken, B. D., Sargent, M. A., Prasad, V., Valiente-Alandi, I., Blaxall, B. C., & Molkentin, J. D. (2018). Specialized fibroblast differentiated states underlie scar formation in the infarcted mouse heart. Journal of Clinical Investigation, 128(5), 2127-2143. https://doi.org/10.1172/jci98215

23. Fujita, B., & Zimmermann, W.-H. (2017). Engineered Heart Repair. Clinical Pharmacology & Therapeutics, 102(2), 197-199. https://doi.org/10.1002/cpt.724

24. Gonzales, A. L., Klug, N. R., Moshkforoush, A., Lee, J. C., Lee, F. K., Shui, B., Tsoukias, N. M., Kotlikoff, M. I., Hill-Eubanks, D., & Nelson, M. T. (2020). Contractile pericytes determine the direction of blood flow at capillary junctions. Proceedings of the National Academy of Sciences, 117(43), 27022-27033. https://doi.org/10.1073/pnas.1922755117

25. Hamilton, N. B. (2010). Pericyte-mediated regulation of capillary diameter: a component of neurovascular coupling in health and disease. Frontiers in Neuroenergetics, 2. https://doi.org/10.3389/fnene.2010.00005

26. Han, K.-Y., Chang, J.-H., Lee, H., & Azar, D. T. (2016). Proangiogenic Interactions of Vascular Endothelial MMP14 With VEGF Receptor 1 in VEGFA-Mediated Corneal Angiogenesis. Investigative Opthalmology & Visual Science, 57(7), 3313. https://doi.org/10.1167/iovs.16-19420

27. Hsieh, P. C. H., Davis, M. E., Lisowski, L. K., & Lee, R. T. (2006). ENDOTHELIAL-CARDIOMYOCYTE INTERACTIONS IN CARDIAC DEVELOPMENT AND REPAIR. Annual Review of Physiology, 68(1), 51-66. https://doi.org/10.1146/annurev.physiol.68.040104.124629

28. Khan, M. A., Hashim, M. J., Mustafa, H., Baniyas, M. Y., Al Suwaidi, S. K. B. M., Alkatheeri, R., Alblooshi, F. M. K., Almatrooshi, M. E. A. H., Alzaabi, M. E. H., Al Darmaki, R. S., & Lootah, S. N. A. H. (2020). Global Epidemiology of Ischemic Heart Disease: Results from the Global Burden of Disease Study. Cureus. https://doi.org/10.7759/cureus.9349

29. Kim, J. S., Park, S. W., Hwang, I., Kim, Y. W., Kim, J. H., & Kim, J. H. (2015). Expression of nestin on endothelial cells and pericytes during vascular development in mouse retina. Investigative ophthalmology & visual science., 56(7), 3403.
30. Kisler, K., Nikolakopoulou, A. M., Sweeney, M. D., Lazic, D., Zhao, Z., & Zlokovic, B. V. (2020). Acute Ablation of Cortical Pericytes Leads to Rapid Neurovascular Uncoupling. Front Cell Neurosci, 14, 27. https://doi.org/10.3389/fncel.2020.00027
31. Konstantin Stark, K. P., Steffen Massberg. (2018). Role of pericytes in vascular immunosurveillance. Frontiers In Bioscience-Landmark, 23(4), 767-781. https://doi.org/10.2741/4615
32. Lee, L. L., Khakoo, A. Y., & Chintalgattu, V. (2019). Isolation and Purification of Murine Cardiac Pericytes. Journal of Visualized Experiments (150). https://doi.org/10.3791/59571
33. Lee, L. L., Khakoo, A. Y., & Chintalgattu, V. (2021). Cardiac pericytes function as key vasoactive cells to regulate homeostasis and disease. FEBS Open Bio, 11(1), 207-225. https://doi.org/10.1002/2211-5463.13021
34. Levine, A. J. (1997). p53, the Cellular Gatekeeper for Growth and Division. Cell, 88(3), 323-331. https://doi.org/10.1016/s0092-8674(00)81871-1
35. Lupu, I.-E., De Val, S., & Smart, N. (2020). Coronary vessel formation in development and disease: mechanisms and insights for therapy. Nature Reviews Cardiology, 17(12), 790-806. https://doi.org/10.1038/s41569-020-0400-1
36. Lupu, I.-E., Redpath, A. N., & Smart, N. (2020). Spatiotemporal Analysis Reveals Overlap of Key Proepicardial Markers in the Developing Murine Heart. Stem Cell Reports, 14(5), 770-787. https://doi.org/10.1016/j.stemcr.2020.04.002

37. Muhl, L., Genové, G., Leptidis, S., Liu, J., He, L., Mocci, G., Sun, Y., Gustafsson, S., Buyandelger, B., Chivukula, I. V., Segerstolpe, Å., Raschperger, E., Hansson, E. M., Björkegren, J. L. M., Peng, X.-R., Vanlandewijck, M., Lendahl, U., & Betsholtz, C. (2020). Single-cell analysis uncovers fibroblast heterogeneity and criteria for fibroblast and mural cell identification and discrimination. Nature Communications, 11(1). https://doi.org/10.1038/s41467-020-17740-1

38. Murray, I. R., Baily, J. E., Chen, W. C. W., Dar, A., Gonzalez, Z. N., Jensen, A. R., Petrigliano, F. A., Deb, A., & Henderson, N. C. (2017). Skeletal and cardiac muscle pericytes: Functions and therapeutic potential. Pharmacology & Therapeutics, 171, 65-74. https://doi.org/10.1016/j.pharmthera.2016.09.005

39. O'Farrell, F. M., & Attwell, D. (2014). A role for pericytes in coronary no-reflow. Nature Reviews Cardiology, 11(7), 427-432. https://doi.org/10.1038/nrcardio.2014.58

40. O'Farrell, F. M., Mastitskaya, S., Hammond-Haley, M., Freitas, F., Wah, W. R., & Attwell, D. (2017). Capillary pericytes mediate coronary no-reflow after myocardial ischaemia. eLife, 6. https://doi.org/10.7554/elife.29280

41. Orlich, M. M., Diéguez-Hurtado, R., Muehlfriedel, R., Sothilingam, V., Wolburg, H., Oender, C. E., Woelffing, P., Betsholtz, C., Gaengel, K., Seeliger, M., Adams, R. H., & Nordheim, A. (2022). Mural Cell SRF Controls Pericyte Migration, Vessel Patterning and Blood Flow. Circulation Research, 131(4), 308-327. https://doi.org/10.1161/circresaha.122.321109

42. Payan, S. M., Hubert, F., & Rochais, F. (2020). Cardiomyocyte proliferation, a target for cardiac regeneration. Biochim Biophys Acta Mol Cell Res, 1867(3), 118461. https://doi.org/10.1016/j.bbamcr.2019.03.008

43. Pham, T. T. D., Park, S., Kolluri, K., Kawaguchi, R., Wang, L. J., Tran, D., Zhao, P., Carmichael, S. T., & Ardehali, R. (2021). Heart and Brain Pericytes Exhibit a Pro-Fibrotic Response After Vascular Injury. Circulation Research, 129(7), E141-E143. https://doi.org/10.1161/Circresaha.121.319288

44. Pomara, C., Bello, S., Neri, M., Riezzo, I., Fineschi, V., Turillazzi, E., Pomara, C., Bello, S., Neri, M., Riezzo, I., & Fineschi, V. (2015). The Meaning of Different Forms of Structural Myocardial Injury, Immune Response and Timing of Infarct Necrosis and Cardiac Repair. Current Vascular Pharmacology, 13(1), 6-19. https://doi.org/10.2174/15701611113119990008

45. Prabhu, S. D., & Frangogiannis, N. G. (2016). The Biological Basis for Cardiac Repair After Myocardial Infarction. Circulation Research, 119(1), 91-112. https://doi.org/10.1161/circresaha.116.303577

46. Quijada, P., Park, S., Kolluri, K., Wong, D., Shih, K. D., Fang, K., et al. (2022). Cardiac Pericytes Mediate the Fibrotic Remodeling Response to Myocardial Infarction. Manuscript in Review at the Journal of Clinical Investigation.

47. Quijada, P., Trembley, M. A., & Small, E. M. (2020). The Role of the Epicardium During Heart Development and Repair. Circulation Research, 126(3), 377-394. https://doi.org/10.1161/circresaha.119.315857

48. Rubin, S. A., Fishbein, M. C., & Swan, H. J. C. (1983). Compensatory hypertrophy in the heart after myocardial infarction in the rat. Journal of the American College of Cardiology, 1(6), 1435-1441. https://doi.org/10.1016/S0735-1097(83)80046-1

49. Sharma, B., Chang, A., & Red-Horse, K. (2017). Coronary Artery Development: Progenitor Cells and Differentiation Pathways. Annual Review of Physiology, 79(1), 1-19. https://doi.org/10.1146/annurev-physiol-022516-033953

50. Sounni, N. E., Dehne, K., Van Kempen, L., Egeblad, M., Affara, N. I., Cuevas, I., Wiesen, J., Junankar, S., Korets, L., Lee, J., Shen, J., Morrison, C. J., Overall, C. M., Krane, S. M., Werb, Z., Boudreau, N., & Coussens, L. M. (2010). Stromal regulation of vessel stability by MMP14 and TGFβ. Disease Models & Mechanisms, 3(5-6), 317-332. https://doi.org/10.1242/dmm.003863

51. Stevens, J. R., Zamani, A., Osborne, J. I. A., Zamani, R., & Akrami, M. (2021). Critical evaluation of stents in coronary angioplasty: a systematic review. BioMedical Engineering OnLine, 20(1). https://doi.org/10.1186/s12938-021-00883-7

52. Su, H., Cantrell, A. C., Zeng, H., Zhu, S.-H., & Chen, J.-X. (2021). Emerging Role of Pericytes and Their Secretome in the Heart. Cells, 10(3), 548. https://doi.org/10.3390/cells10030548

53. Su, T., Stanley, G., Sinha, R., D'Amato, G., Das, S., Rhee, S., Chang, A. H., Poduri, A., Raftrey, B., Dinh, T. T., Roper, W. A., Li, G., Quinn, K. E., Caron, K. M., Wu, S., Miquerol, L., Butcher, E. C., Weissman, I., Quake, S., & Red-Horse, K. (2018). Single-cell analysis of early progenitor cells that build coronary arteries. Nature, 559(7714), 356-362. https://doi.org/10.1038/s41586-018-0288-7

54. Tucker, N. R., Chaffin, M., Fleming, S. J., Hall, A. W., Parsons, V. A., Bedi, K. C., Akkad, A.-D., Herndon, C. N., Arduini, A., Papangeli, I., Roselli, C., Aguet, F., Choi, S. H., Ardlie, K. G., Babadi, M., Margulies, K. B., Stegmann, C. M., & Ellinor, P. T. (2020).

Transcriptional and Cellular Diversity of the Human Heart. Circulation, 142(5), 466-482. https://doi.org/10.1161/circulationaha.119.045401

55. Varshney, R., Ranjit, R., Chiao, Y. A., Kinter, M., & Ahn, B. (2021). Myocardial Hypertrophy and Compensatory Increase in Systolic Function in a Mouse Model of Oxidative Stress. International Journal of Molecular Sciences, 22(4), 2039. https://doi.org/10.3390/ijms22042039
56. Volz, K. S., Jacobs, A. H., Chen, H. I., Poduri, A., Mckay, A. S., Riordan, D. P., Kofler, N., Kitajewski, J., Weissman, I., & Red-Horse, K. (2015). Pericytes are progenitors for coronary artery smooth muscle. eLife, 4. https://doi.org/10.7554/elife.10036
57. Wang, Z., Cui, M., Shah, A. M., Tan, W., Liu, N., Bassel-Duby, R., & Olson, E. N. (2020). Cell-Type-Specific Gene Regulatory Networks Underlying Murine Neonatal Heart Regeneration at Single-Cell Resolution. Cell Reports, 33(10), 108472. https://doi.org/10.1016/j.celrep.2020.108472
58. Wu, Y., Zhou, L., Liu, H., Duan, R., Zhou, H., Zhang, F., He, X., Lu, D., Xiong, K., Xiong, M., Zhuang, J., Liu, Y., Li, L., Liang, D., & Chen, Y.-H. (2021). LRP6 downregulation promotes cardiomyocyte proliferation and heart regeneration. Cell Research, 31(4), 450-462. https://doi.org/10.1038/s41422-020-00411-7
59. Xiaojuan Su, L. H., Yi Qu, Dongqiong Xiao, and Dezhi Mu. (2019). Pericytes in Cerebrovascular Diseases: An Emerging Therapeutic Target. Frontiers in Cellular Neuroscience, 13. https://doi.org/10.3389/fncel.2019.00519
60. Xin, M., Olson, E. N., & Bassel-Duby, R. (2013). Mending broken hearts: cardiac development as a basis for adult heart regeneration and repair. Nature Reviews Molecular Cell Biology, 14(8), 529-541. https://doi.org/10.1038/nrm3619

61. Yamamoto, S., Muramatsu, M., Azuma, E., Ikutani, M., Nagai, Y., Sagara, H., Koo, B.-N., Kita, S., O'Donnell, E., Osawa, T., Takahashi, H., Takano, K.-I., Dohmoto, M., Sugimori, M., Usui, I., Watanabe, Y., Hatakeyama, N., Iwamoto, T., Komuro, I., . . . Sasahara, M. (2017). A subset of cerebrovascular pericytes originates from mature macrophages in the very early phase of vascular development in CNS. Scientific Reports, 7(1). https://doi.org/10.1038/s41598-017-03994-1

62. Yang, L., Deng, J., Ma, W., Qiao, A., Xu, S., Yu, Y., Boriboun, C., Kang, X., Han, D., Ernst, P., Zhou, L., Shi, J., Zhang, E., Li, T.-S., Qiu, H., Nakagawa, S., Blackshaw, S., Zhang, J., & Qin, G. (2021). Ablation of lncRNA Miat attenuates pathological hypertrophy and heart failure. Theranostics, 11(16), 7995-8007. https://doi.org/10.7150/thno.50990

63. Zhao, G., Joca, H. C., Nelson, M. T., & Lederer, W. J. (2020). ATP- and voltage-dependent electro-metabolic signaling regulates blood flow in heart. Proceedings of the National Academy of Sciences, 117(13), 7461-7470. https://doi.org/10.1073/pnas.1922095117

64. Zhao, H., & Chappell, J. C. (2019). Microvascular bioengineering: a focus on pericytes. Journal of Biological Engineering, 13(1). https://doi.org/10.1186/s13036-019-0158-3

65. Zhao, T., Kee, H. J., Bai, L., Kim, M.-K., Kee, S.-J., & Jeong, M. H. (2021). Selective HDAC8 inhibition attenuates isoproterenol-induced cardiac hypertrophy and fibrosis via p38 MAPK pathway. Frontiers in pharmacology, 12, 677757.